UNIVERSITY OF
BATH

Link to publication

University of Bath

.

SPATIALLY-RESOLVED DUST MAPS FROM BALMER DECREMENTS IN GALAXIES AT $Z \sim 1.4$

Erica June Nelson[1], Pieter G. van Dokkum[1], Ivelina G. Momcheva[2], Gabriel B. Brammer[2], Stijn Wuyts[3], Marijn Franx[4], Natascha M. Förster Schreiber[5], Katherine E. Whitaker[6†], Rosalind E. Skelton[7]

Submitted to ApJ Letters

ABSTRACT

We derive average radial gradients in the dust attenuation towards H II regions in 609 galaxies at $z \sim 1.4$, using measurements of the Balmer decrement out to $r \sim 3$ kpc. The Balmer decrements are derived from spatially resolved maps of Hα and Hβ emission from the 3D-HST survey. We find that with increasing stellar mass M$_*$ both the normalization and strength of the gradient in dust attenuation increases. Galaxies with a mean mass of $\langle \log M \rangle = 9.2$ M$_\odot$ have little dust attenuation at all radii, whereas galaxies with $\langle \log M \rangle = 10.2$ M$_\odot$ have $A_{\mathrm{H}\alpha} \approx 2$ mag in their central regions. We parameterize this as $A_{\mathrm{H}\alpha} = b + c \log r$, with $b = 0.9 + 1.0 \log M_{10}$, $c = -1.9 - 2.2 \log M_{10}$, r in kpc, and M_{10} the stellar mass in units of 10^{10} M$_\odot$. This expression can be used to correct spatially resolved measurements of Hα to radial distributions of star formation. When applied to our data, we find that the star formation rates in the central $r < 1$ kpc of galaxies in the highest mass bin are ~ 6 M$_\odot$ yr^{-1}, six times higher than before correction and approximately half of the total star formation rate of these galaxies. If this high central star formation rate is maintained for several Gyr, a large fraction of the stars in present-day bulges likely formed in-situ.

Subject headings: galaxies: dust attenuation — galaxies: evolution — galaxies: structure — galaxies: star formation

1. INTRODUCTION

In the local Universe, the star formation surface density is determined by the molecular gas surface density (e.g. Larson 1992). Recent studies have shown that this relation probably holds at higher redshift ($1 < z < 3$) as well (e.g. Tacconi et al. 2013; Genzel et al. 2015), suggesting that the gas reservoir is the key factor controlling the growth rate of galaxies. In the broader context of galaxy evolution, this has been interpreted as evidence for the equilibrium growth framework in which star formation is regulated by a balance between inflows and outflows (Bouché et al. 2010; Davé, Finlator, & Oppenheimer 2012; Lilly et al. 2013; Peng & Maiolino 2014). In this model, galaxy growth in an integrated sense is driven by the cycle of baryons between galaxies and the halo gas (Davé et al. 2012) with the star formation efficiency set by stellar feedback (Hopkins et al. 2014).

However, in a resolved sense, exactly how different physical processes couple in different parts of galaxies to regulate star formation and drive structural assembly remains unknown (Davé et al. 2012). Observationally, significant progress is being made in mapping the molecular gas reservoir and the spatial distribution of star formation of galaxies. Molecular gas can now be mapped based on the spatial distribution of CO thanks to millimeter arrays such as PdB and ALMA (e.g. Genzel et al. 2013; Rybak et al. 2015). Star for-

mation can be mapped out to $z \sim 2.5$ using the spatial distribution of the Hα emission line owing to integral field units on ground-based telescopes (SINFONI, OSIRIS, KMOS Förster Schreiber et al. 2009; Law et al. 2009; Wisnioski et al. 2015) and the WFC3 grism on HST (Nelson et al. 2012; Nelson et al. 2013).

However, studies of spatially resolved star formation using the Hα emission line suffer from an important systematic uncertainty as they only trace the photons that are not absorbed by dust. The dust attenuation toward star-forming regions is most directly probed using Balmer recombination line flux ratios, the Balmer decrement: as dust attenuation is wavelength dependent, its effects can be measured by comparing the observed and intrinsic Balmer decrements (e.g. Calzetti 1997). On a galaxy-integrated basis, the quantity of dust attenuation toward HII regions ($A_{\mathrm{H}\alpha}$) measured using Balmer decrements has been shown to increase with increasing stellar mass (M$_*$), star formation rate (SFR), and attenuation toward the stars (A_v) (Calzetti et al. 2000; Wild et al. 2011; Momcheva et al. 2013; Domínguez et al. 2013; Price et al. 2014; Reddy et al. 2015). As the stellar mass surface density and the star formation surface density are typically highest in the centers of galaxies, we expect the attenuation to vary within galaxies, such that the dust attenuation is highest in the centers. This is also expected from the fact that both the metallicity and, most importantly, the gas column density increase with decreasing distance from the center (e.g. Bohlin, Savage, & Drake 1978; Gilli et al. 2014; Nelson et al. 2014). Therefore, in order to tie the global gas reservoir to galactic structural assembly we need to correct the spatially-resolved Hα measurements for the attenuation toward star-forming regions.

Measuring spatially-resolved Balmer decrements is now possible with the Wide Field Camera 3 (WFC3) grism capability on the Hubble Space Telescope, which we employed for the 3D-HST survey (Brammer et al. 2012; Momcheva et al. 2015). The grism data enable us to create emission line maps for every object in the survey (see Nelson et al. 2012; Nel-

[1] Astronomy Department, Yale University, New Haven, CT 06511, USA
[2] Space Telescope Science Institute, 3700 San Martin Drive, Baltimore, MD 21218, USA
[3] Department of Physics, University of Bath, Claverton Down, Bath, BA2 7AY, UK
[4] Leiden Observatory, Leiden University, Leiden, The Netherlands
[5] Max-Planck-Institut für extraterrestrische Physik, Giessenbachstrasse, D-85748 Garching, Germany
[6] Department of Astronomy, University of Massachusetts, Amherst, MA 01003, USA
[7] South African Astronomical Observatory, P.O. Box 9, Observatory, 7935, South Africa
† Hubble Fellow

son et al. 2013; Wuyts et al. 2013; Nelson et al. 2015). In a narrow redshift window ($1.35 < z < 1.5$) we can map the spatial distribution of both the Hα and Hβ emission lines, as they both fall within the G141 wavelength coverage. Galaxy-integrated Balmer decrements were analyzed in Price et al. (2014).

Here we present spatially resolved Balmer decrements for galaxies at $z \sim 1.4$ and derive radial dust gradients. The gradients are measured from deep stacks, using the full 3D-HST dataset. We study radial dust gradients as a function of M_*, and apply these gradients to the observed Hα distributions to obtain spatially-resolved dust-corrected star formation surface density profiles.

2. SPATIALLY-RESOLVED BALMER DECREMENTS

We use data from the 3D-HST survey, a 248 orbit NIR slit-less spectroscopic survey over the CANDELS fields with the G141 grism (Brammer et al. 2012; Skelton et al. 2014; Momcheva et al. 2015). These slitless grism observations have high spatial resolution and low spectral resolution, and therefore provide images of galaxies in the light of their emission lines for every object in the field of view. We focus on the redshift range $1.35 < z < 1.5$, for which both Hα and Hβ fall in the wavelength coverage of the G141 grism. The absence of sky emission lines in the spectra implies that no further restrictions on the redshifts are required; in ground-based observations it is rare that both Hα and Hβ are unaffected by OH lines. The galaxies are divided in three mass bins: $[9.0 \leq M_* < 9.2]$, $[9.2 \leq M_* < 9.8]$, $[9.8 \leq M_* < 11.0]$, The median stellar mass in these bins is 9.17, 9.53, and 10.23 respectively.

A detailed description of how emission line maps are made from grism data is provided in Nelson et al. (2015). Briefly, the Hα and Hβ emission line maps are made by subtracting the continuum from the two-dimensional spectra and masking contaminating flux from nearby objects. We stack the Hα and Hβ emission line maps as a function of M_*. These properties were determined from the combination of the grism spectra and deep UV-IR photometric catalogs (Brammer et al. 2012; Skelton et al. 2014; Whitaker et al. 2014). We select all galaxies with $H_{F140W} \leq 24$, applying no emission line flux limit for Hα or Hβ so as not to introduce systematics into the line ratio measurements. Galaxies which have Hα or Hβ emission line maps with more than half of their central 3 kpc masked due to contamination are removed; this is roughly half of the sample. In the stacking procedure the broadband H_{F140W} emission is used to center and normalize the emission line maps. We masked the nearby [S II] $\lambda\lambda6716, 6731$Å and [O III] $\lambda\lambda4959, 5007$ lines with an asymmetric double pac-man mask (see Nelson et al. 2015). We correct the image stacks for the effects of the point spread function (PSF), using the method described in Szomoru et al. (2013) and Nelson et al. (2015): after fitting the stacks with GALFIT (Peng et al. 2010), the residuals of the fit are added to the unconvolved GALFIT Sérsic model.[‡] This method has been shown to reconstruct the true flux distribution even if the Sérsic model is a poor fit (Szomoru et al. 2013). The averaged maps are shown in Fig. 1. Radial profiles of the Hα and Hβ emission are computed in circular apertures, again following Nelson et al. (2015).
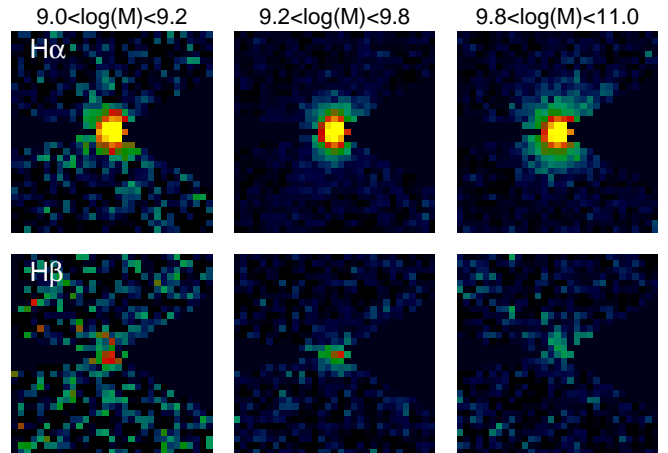
FIG. 1.— Averaged maps of Hα and Hβ emission, in three different stellar mass bins. These maps were obtained by stacking continuum-subtracted two-dimensional spectra of galaxies at $1.35 \leq z \leq 1.53$ from the 3D-HST survey.

We correct these measured profiles for [N II] emission. As a result of the low spectral resolution of the G141 grism, [N II] $\lambda6548, 6583$ and Hα $\lambda6563$ are blended in our spectra. To account for the contamination of Hα by [N II], the blended observed line must be scaled by a factor Hα_{corr} =Hα_{meas}/(1+[N II]/Hα). We cannot measure [N II]/Hα directly, and we make use of previous measurements in the literature. The galaxy-integrated [N II]/Hα increases as a function of M_* (e.g. Erb et al. 2006; Zahid et al. 2014; Steidel et al. 2014; Wuyts et al. 2014), which is probably a reflection of the mass-metallicity relation. We use the Zahid et al. (2014) relation and scale the overall normalization of the radial Hα profiles down accordingly. The adopted [N II]/Hα ratios are [0.03,0.07,0.24] for the low through high mass stacks respectively.

We also consider the effects of gradients in [N II]/Hα within the galaxies, as abundance gradients have been widely observed in the local Universe (e.g. Sánchez et al. 2014). However, trends at higher redshift are much less certain with observed [N II]/Hα gradients ranging from flat or negative to positive (Swinbank et al. 2012; Jones et al. 2013; Stott et al. 2014,Leethochawalit et al. 2015, Wuyts et al. in prep). Given these uncertainties we do not apply a radially-varying correction, but we note that adopting a radial gradient of [N II]/Hα= -0.18 dex/r_e, as inferred from radial O/H measurements in the local Universe (Sánchez et al. 2014), does not change our results.

Typically, Balmer emission lines also need to be corrected for underlying absorption. The atmospheres of stars (particularly A stars) produce Balmer absorption lines and the emission line flux must first fill in the absorption. In our analysis, the absorption was corrected for in the subtraction of the two-dimensional continuum model. This model is a linear combination of EAzY templates with emission lines removed (see Brammer, van Dokkum, & Coppi 2008; Momcheva et al. 2015) which is then convolved with the $J_{F125W}/H_{F140W}/H_{F160W}$ detection image. Therefore, the continuum model has, to very good approximation, both the same spectrum and morphology as the true continuum emission that underlies our emission line maps. We are essentially subtracting a negative image of the galaxy in absorption. For reference, the integrated absorption line strength is $\sim 2 - 3.5$ Å
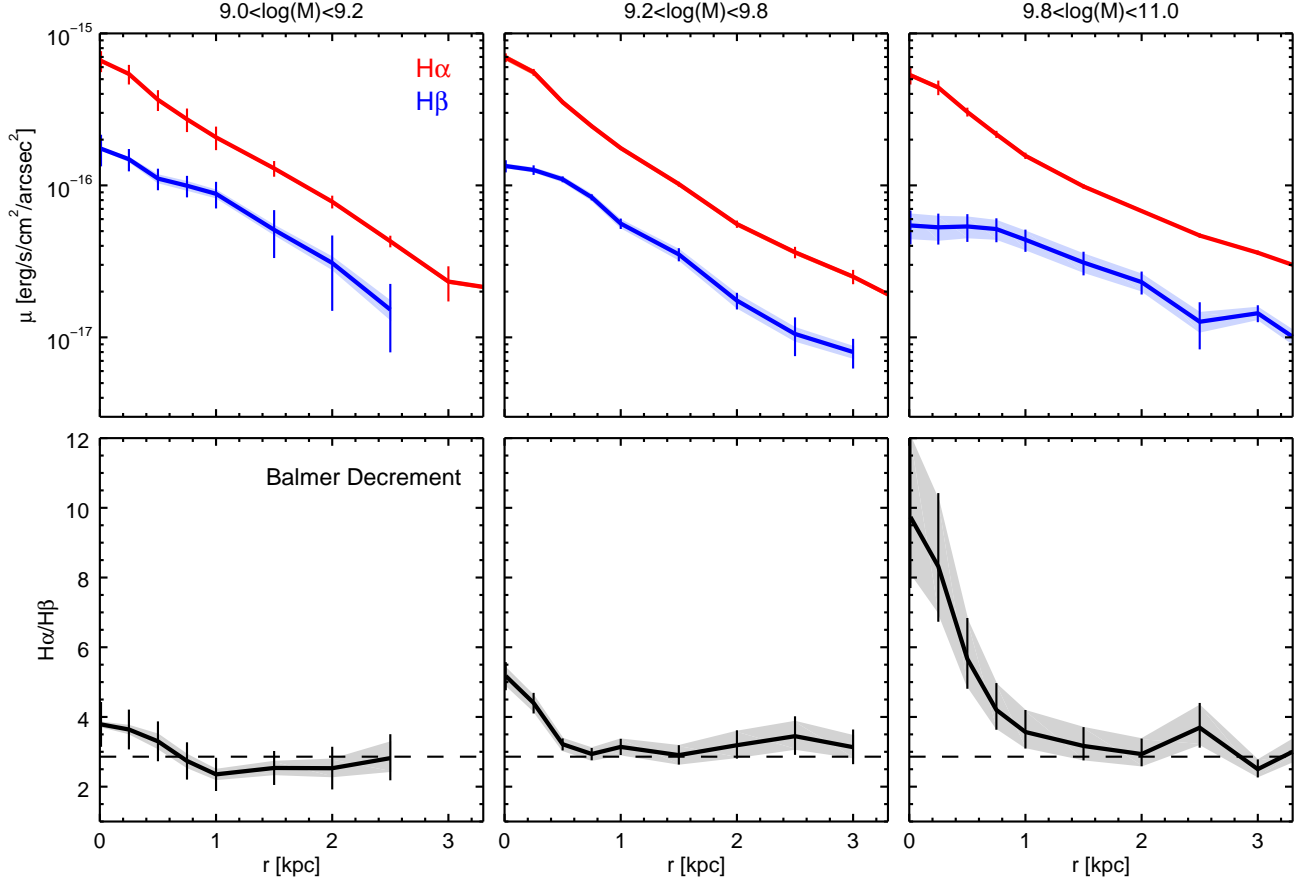
FIG. 2.— Average radial surface brightness profiles of Hα (red), Hβ (blue), and Hα/Hβ (the Balmer decrement, black) in galaxies as a function of M∗. Random uncertainties are shown by bootstrap error bars. Systematic uncertainties derived by artificially increasing and decreasing the absorption line equivalent widths by half are shown by shaded regions. The dashed line shows (Hα/Hβ)$_{int}$, the 'intrinsic' line ratio in the absence of dust attenuation. We can reliably measure the average Balmer decrement gradients in galaxies at $z \sim 1.4$ to nearly 3 kpc. With the Balmer decrement tracing dust attenuation toward H II regions, this figure shows that with increasing stellar mass, galaxies become increasingly dust-obscured toward their centers.

in the stacks, consistent with, e.g., Domínguez et al. (2013); Momcheva et al. (2013). This is, in general, a small fraction of the emission line equivalent width, although it becomes more significant for Hβ at the highest masses (up to $\sim 30\%$).

The fully corrected Hα and Hβ profiles, in units of erg s^{-1} cm^{-2} arcsec^{-2}, are shown in Fig. 2. We can reliably trace Hα out to $\gtrsim 6$ kpc, and the $\gtrsim 3\times$ fainter Hβ out to ~ 3 kpc; at larger radii the error in the measurement is more than half of the measured flux. At low masses, the Hα and Hβ surface brightness profiles are nearly exponential. As mass increases, the Hα emission grows more centrally concentrated while the Hβ becomes *less* centrally concentrated than exponential. This is the central result of this Letter: with increasing stellar mass, galaxies become increasingly more dust obscured toward their centers.

Fig. 2 also shows the effect of assuming different quantities of stellar absorption (shaded regions). These profiles were derived by artificially changing the absorption line equivalent width in the best-fitting 2D EAzY model, increasing and decreasing it by half.

3. RADIAL GRADIENTS IN DUST ATTENUATION

The increase in the slope and normalization of the Balmer decrement with M∗ implies a corresponding increase in the slope and normalization of the dust attenuation. We derive

the dust attenuation toward Hα as follows. The increase of the Balmer decrement over the intrinsic value can be expressed in terms of a Balmer color excess:

$$E(H\beta - H\alpha) = 2.5 \log \left(\frac{(H\alpha/H\beta)_{obs}}{(H\alpha/H\beta)_{int}} \right) \quad (1)$$

Here (Hα/Hβ)$_{int}$ is the expected ratio produced by the recombination and subsequent cascade of electrons in photoionized hydrogen atoms: (Hα/Hβ)$_{int} = 2.86$ for Case B recombination and $T = 10^4$K (Osterbrock & Ferland 2006).

If dust is present, it will preferentially attenuate the shorter wavelength Hβ λ4861Å more than the longer wavelength Hα λ6563Å, increasing the observed value of the Balmer decrement ((Hα/Hβ)$_{obs}$). The Balmer color excess can therefore be used to derive the attenuation toward Hα:

$$A_{H\alpha} = \frac{E(H\beta - H\alpha)}{k(\lambda_{H\beta}) - k(\lambda_{H\alpha})} \times k(\lambda_{H\alpha}) \quad (2)$$

Deriving $A_{H\alpha}$ requires the adoption of a reddening curve $k(\lambda)$ to compute the values at Hα ($k(\lambda_{H\alpha})$) and Hβ ($k(\lambda_{H\beta})$).

In Fig. 3 we show the radial trend of the absorption toward Hα, $A_{H\alpha}$ using different parameterizations of the reddening and attenuation. As expected from the trends in the Balmer decrement profiles, $A_{H\alpha}$ shows a stronger dependence on ra-
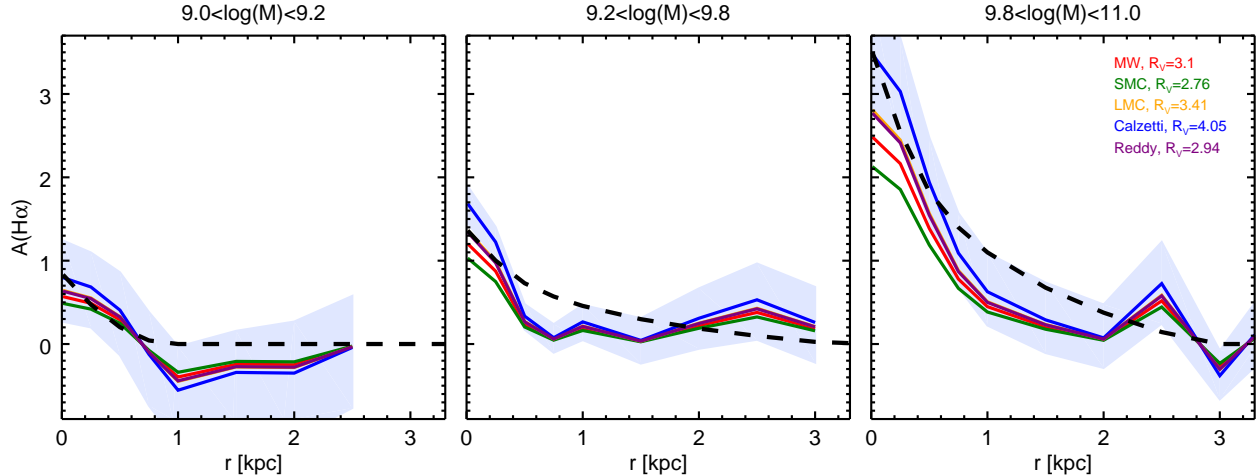
FIG. 3.— Radial profiles of dust attenuation toward the Hα emission line ($A_{H\alpha}$) in galaxies as a function of M$_*$. $A_{H\alpha}$ is computed by scaling the Balmer decrement using a dust law. Different dust laws result in different conversions from the radial Balmer decrement profiles in the previous figure to the $A_{H\alpha}$ profiles here, shown in different colors. (Calzetti et al. 2000; Gordon et al. 2003; Reddy et al. 2015). In summary, the star formation in the centers of galaxies becomes more obscured with increasing stellar mass.

dius and a higher overall normalization for higher masses. The attenuation in low mass galaxies is essentially zero at all radii. As mass increases, attenuation increases toward the center. In the highest mass bin, the attenuation in the central regions reaches values in excess of two magnitudes.

While the qualitative trends remain unchanged with different dust laws, the profiles do have quantitative differences. In particular, $A_{H\alpha}$ is higher if the slope of the attenuation curve is flatter between the wavelengths of Hα and Hβ or if R_V is larger (see e.g. Cardelli, Clayton, & Mathis 1989; Calzetti et al. 2000; Gordon et al. 2003; Reddy et al. 2015). With the exception of the centers of the highest mass galaxies, these differences are small compared to the systematic and random errors in the measurements of the Balmer decrement.

We quantify the radial dust profiles as follows:

$$A_{H\alpha} = b + c \log r, \tag{3}$$

with r in kpc. We fit the dust profiles derived using the Calzetti et al. (2000) attenuation curve, for consistency with previous work (e.g. Momcheva et al. 2013; Domínguez et al. 2013; Price et al. 2014) and because this curve gives the best agreement with the total UV+IR star formation rates (see Sect. 4). For the three mass bins we find $b = [0.0, 0.46, 1.10]$ and $c = [0.0, -0.90, -2.40]$. We set b and c to zero in the lowest mass bin as the formal best fit is (slightly) negative. These fits are shown by the thick dashed lines in Fig. 3. While the observed profiles show hints of more complex structure, perhaps even separate bulge and disk components, higher order fits are not justified given the low signal-to-noise ratio and the spatial resolution of the data.

We parameterize the change of the slope and normalization with M$_*$ by fitting linear functions to the coefficients $b(M)$ and $c(M)$. To good approximation (± 0.05 mag), we find $b = 0.9 + 1.0 \log M_{10}$ and $c = -1.9 - 2.2 \log M_{10}$, with M_{10} the stellar mass in units of 10^{10} M$_\odot$. Over a decade in mass, the attenuation at 2 kpc increases by ~ 0.5 magnitudes, and the attenuation at 0.5 kpc increases by ~ 1.5 magnitudes. The gradients are consistent with the galaxy-integrated measurements of Price et al. (2014).

4. DUST-CORRECTED RADIAL PROFILES OF STAR FORMATION

With the radial profiles of Hα and $A_{H\alpha}$, we derive radial profiles of star formation corrected for dust. Star formation rates are computed from Hα emission using Kennicutt (1998) and a Chabrier (2003) initial mass function:

$$SFR(H\alpha) = 4.68 \times 10^{-42} L_{H\alpha} \tag{4}$$

Star formation rates are corrected for the dust attenuation toward HII regions ($A_{H\alpha}$) using:

$$SFR(dust\,corrected) = SFR(H\alpha) \times \exp(A_{H\alpha}/1.086), \tag{5}$$

with $A_{H\alpha}$ given by Eq. 3.

Figure 4 shows the radial SFR profiles corrected for dust. As a test of our procedure, we integrate these dust-corrected SFR profiles out to $r = 2r_e$ (with r_e the half light radius of the H_{F140W} emission), and compare them to the average UV+IR star formation rates of the same galaxies (see Whitaker et al. 2014; Momcheva et al. 2015). In the three mass bins, we find that the total Hα-derived star formation rates are 2.4, 3.3, and 8.6 respectively. The ratios of the Hα star formation rates to the UV+IR star formation rates are 1.3, 1.2, and 0.7 respectively. These ratios are similar when using the Whitaker et al. (2014) UV+IR SFR measurements for the median masses in the bins. We conclude that the dust corrections are reasonable to within the systematic uncertainty of our UV+IR star formation rates (see e.g. Utomo et al. 2014).[§]

Particularly in our highest mass bin the implied central SFRs are much higher than prior to the dust correction: the total star formation in the central $r < 1$ kpc is $5.6\,M_\odot$/yr in the highest mass bin, whereas it was $0.9\,M_\odot$/yr before correction. Approximately half of the total star formation rate takes place inside 1 kpc in the highest mass bin.

5. DISCUSSION

Using the WFC3 grism to map the distribution of Hα and Hβ emission, we constructed the first spatially-resolved maps

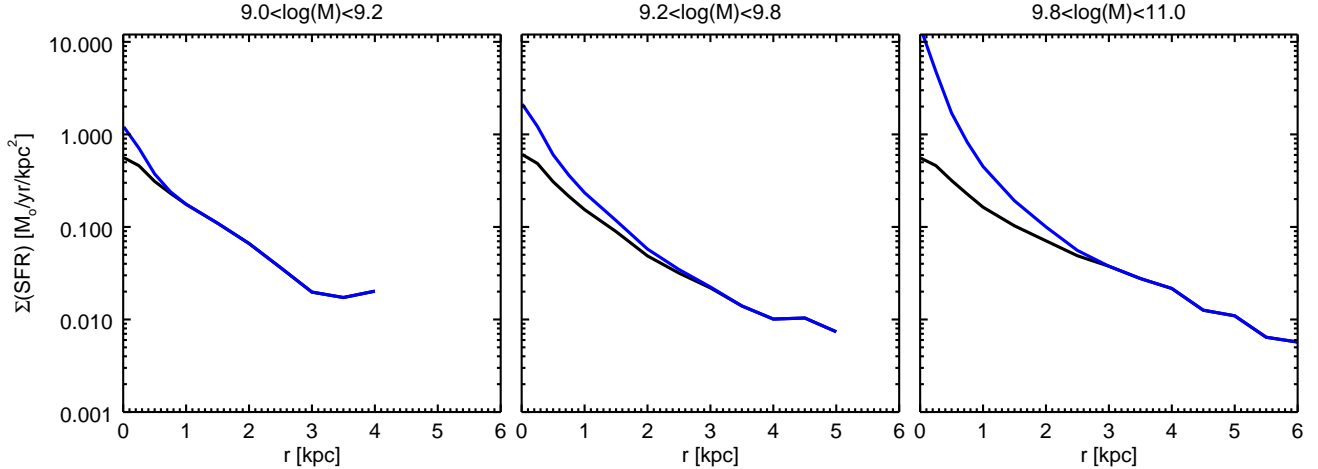§ The small discrepancy in the highest mass bin could be due to star formation with very high optical depth.

FIG. 4.— Radial profiles of SFR determined directly from Hα emission are shown in black, radial profiles of SFR corrected for dust using radial Balmer decrement profiles are shown in blue. The excess SFR over an exponential toward the center of high mass galaxies suggests we are witnessing the growth of galactic bulges through in-situ star formation.

of the Balmer decrement at $z > 1$. These measurements provide stringent constraints on the radial gradients in the dust attenuation toward star forming regions of galaxies, allowing us to derive dust-corrected radial distributions of star formation. We find that the dust attenuation is small (< 0.5 mag) at all radii in galaxies with $M < 10^{10}\,M_\odot$. Galaxies with higher masses have significant dust attenuation toward their centers. The immediate implication is that the central ($r \lesssim 2$ kpc) observed Hα emission of high mass galaxies should not be directly converted to star formation, and the central surface brightness should not be directly converted to stellar mass density.

A potential concern in this analysis is that by stacking small galaxies with high attenuation and large galaxies with low attenuation, we could infer a radial dust gradient where on an individual galaxy basis, there is none. To test this, we remove all compact galaxies with sizes more than 0.1 and 0.3 dex below the size-mass relation from the stack. In both cases, the qualitative trends remain unchanged meaning the gradients are real, not a byproduct of stacking a heterogeneous sample. Another concern is that weighting galaxies by their H_{F140W} flux biases the stacks toward galaxies with high Hα and Hβ equivalent widths. If galaxies with high equivalent widths have preferentially low dust attenuation, this analysis could underestimate the true dust attenuation at the median mass of the stacks.

A straightforward interpretation of our results is that we see the in-situ building of bulges in massive galaxies at $z = 1.4$. However, a key question is whether this central star formation accounts for a significant fraction of the stars in the central kpc of present-day galaxies. The total amount of stars that are formed in the central kpc can be approximated by

$$M \sim w\,\mathrm{SFR}\,\tau, \qquad (6)$$

with $w \approx 0.6$ a correction for mass loss due to stellar winds (see e.g. Bruzual & Charlot 2003) and τ the duration of the star formation. For $\tau \sim 2$ Gyr (that is, assuming that the current star formation rate is maintained until $z \sim 0.8$), we find that the total mass that is added is $\sim 7 \times 10^9\,M_\odot$, or $\sim 1/3$ of the total mass of the galaxy. If $\tau \lesssim 1$ Gyr the added mass is much less significant. We note that this does not necessarily imply that galaxies are growing "outside-in": this depends on the radial M_*/L profiles (Szomoru et al. 2013) which are driven by gradients in dust and age. This could be tested by deriving mass profiles from the high spatial resolution CANDELS multi-color imaging.

In summary, we infer that it is possible that a central mass concentration is built up through in-situ star formation in the highest mass galaxies, but only if the radial distribution of star formation observed at $z \sim 1.4$ is sustained over several Gyr. This can be tested with spatially-resolved absorption maps at lower redshift, which can be created using adaptive optics or the G102 grism on the WFC3 camera. Furthermore, high resolution imaging of the molecular gas and of the continuum dust emission with ALMA can provide direct information on the presence of large amounts of dust in the centers of massive galaxies at these redshifts. Finally, with future facilities such as JWST our initial study of averaged spatially-resolved Balmer decrements at moderate redshifts can be expanded to higher redshifts and individual galaxies.

REFERENCES

Bohlin, R. C., Savage, B. D., & Drake, J. F. 1978, ApJ, 224, 132
Bouché, N., Dekel, A., Genzel, R., et al. 2010, ApJ, 718, 1001
Brammer, G. B., van Dokkum, P. G., & Coppi, P. 2008, ApJ, 686, 1503
Brammer, G. B., van Dokkum, P. G., Franx, M., et al. 2012, ApJS, 200, 13
Bruzual, G., & Charlot, S. 2003, Monthly Notices of the Royal Astronomical Society, 344, 1000
Calzetti, D. 1997, AJ, 113, 162
Calzetti, D., Armus, L., Bohlin, R. C., et al. 2000, ApJ, 533, 682
Cardelli, J. A., Clayton, G. C., & Mathis, J. S. 1989, ApJ, 345, 245
Chabrier, G. 2003, PASP, 115, 763
Davé, R., Finlator, K., & Oppenheimer, B. D. 2012, MNRAS, 421, 98

Domínguez, A., Siana, B., Henry, A. L., et al. 2013, ApJ, 763, 145
Erb, D. K., Shapley, A. E., Pettini, M., et al. 2006, ApJ, 644, 813
Förster Schreiber, N. M., Genzel, R., Bouché, N., et al. 2009, ApJ, 706, 1364
Genzel, R., Tacconi, L. J., Kurk, J., et al. 2013, ApJ, 773, 68
Genzel, R., Tacconi, L. J., Lutz, D., et al. 2015, ApJ, 800, 20
Gilli, R., Norman, C., Vignali, C., et al. 2014, A&A, 562, A67
Gordon, K. D., Clayton, G. C., Misselt, K. A., Landolt, A. U., & Wolff, M. J. 2003, ApJ, 594, 279
Hopkins, P. F., Kereš, D., Oñorbe, J., et al. 2014, MNRAS, 445, 581
Jones, T., Ellis, R. S., Richard, J., & Jullo, E. 2013, ApJ, 765, 48
Kennicutt, Jr., R. C. 1998, ARA&A, 36, 189

Larson, R. 1992, in Star Formation in Stellar Systems, ed. G. Tenorio-Tagle,
    M. Prieto, & F. Sanchez, 125
Law, D. R., Steidel, C. C., Erb, D. K., et al. 2009, ApJ, 697, 2057
Leethochawalit, N., Jones, T. A., Ellis, R. S., et al. 2015, ArXiv e-prints,
    arXiv:1509.01279
Lilly, S. J., Carollo, C. M., Pipino, A., Renzini, A., & Peng, Y. 2013, ApJ,
    772, 119
Momcheva, I. G., Lee, J. C., Ly, C., et al. 2013, AJ, 145, 47
Momcheva, I. G., Brammer, G. B., van Dokkum, P. G., et al. 2015, ArXiv
    e-prints, arXiv:1510.02106
Nelson, E., van Dokkum, P., Franx, M., et al. 2014, Nature, 513, 394
Nelson, E. J., van Dokkum, P. G., Brammer, G., et al. 2012, ApJ, 747, L28
Nelson, E. J., van Dokkum, P. G., Momcheva, I., et al. 2013, The
    Astrophysical Journal, 763, L16
Nelson, E. J., van Dokkum, P. G., Förster Schreiber, N. M., et al. 2015, ArXiv
    e-prints, arXiv:1507.03999
Osterbrock, D. E., & Ferland, G. J. 2006, Astrophysics of gaseous nebulae
    and active galactic nuclei
Peng, C. Y., Ho, L. C., Impey, C. D., & Rix, H.-W. 2010, The Astronomical
    Journal, 139, 2097
Peng, Y.-j., & Maiolino, R. 2014, MNRAS, 443, 3643

Price, S. H., Kriek, M., Brammer, G. B., et al. 2014, ApJ, 788, 86
Reddy, N. A., Kriek, M., Shapley, A. E., et al. 2015, ArXiv e-prints,
    arXiv:1504.02782
Rybak, M., Vegetti, S., McKean, J. P., Andreani, P., & White, S. D. M. 2015,
    MNRAS, 453, L26
Sánchez, S. F., Rosales-Ortega, F. F., Iglesias-Páramo, J., et al. 2014, A&A,
    563, A49
Skelton, R. E., Whitaker, K. E., Momcheva, I. G., et al. 2014, ApJS,214, 24
Steidel, C. C., Rudie, G. C., Strom, A. L., et al. 2014, ApJ, 795, 165
Stott, J. P., Sobral, D., Swinbank, A. M., et al. 2014, MNRAS, 443, 2695
Swinbank, M., Smail, I., Sobral, D., et al. 2012, eprint arXiv:1206.1867
Szomoru, D., Franx, M., van Dokkum, P. G., et al. 2013, ApJ, 763, 73
Tacconi, L. J., Neri, R., Genzel, R., et al. 2013, ApJ, 768, 74
Utomo, D., Kriek, M., Labbé, I., Conroy, C., & Fumagalli, M. 2014, ApJ,
    783, L30
Whitaker, K. E., Franx, M., Leja, J., et al. 2014, ApJ, 795, 104
Wild, V., Charlot, S., Brinchmann, J., et al. 2011, MNRAS, 417, 1760
Wisnioski, E., Förster Schreiber, N. M., Wuyts, S., et al. 2015, ApJ, 799, 209
Wuyts, E., Kurk, J., Förster Schreiber, N. M., et al. 2014, ApJ, 789, L40
Wuyts, S., Förster Schreiber, N. M., Nelson, E. J., et al. 2013, ApJ, 779, 135
Zahid, H. J., Kashino, D., Silverman, J. D., et al. 2014, ApJ, 792, 75